Polymer Testing 108 (2022) 107496

Contents lists available at ScienceDirect

Polymer Testing

journal homepage: www.elsevier.com/locate/polytest

Vulcanization degree influence on the mechanical properties of Fiber Reinforced Elastomeric Isolators made with reactivated EPDM

A.B. Habieb [a], F. Milani [b], G. Milani [c,*], G. Pianese [c], D. Torrini [c]

[a] Department of Civil Engineering, Institut Teknologi Sepuluh Nopember, Surabaya, Indonesia
[b] Chem. Co Consultant, Occhiobello, RO, Italy
[c] Department of Architecture, Built Environment and Construction Engineering, Politecnico di Milano, Milano, Italy

ARTICLE INFO

Keywords:
Fiber reinforced elastomeric isolator (FREI)
Recycled rubber
Regenerated EPDM
Crosslinking
Vulcanization
Experimental tests and numerical computations

ABSTRACT

Rubber is well known as the basic material for some structural devices, such as seaport fenders and seismic isolators. In practice, to seismically isolate a structure it is necessary to interpose between the foundation and the superstructure a rubber device that increases the period of the superstructure, a feature that allows the structure to be "transparent" to the seismic excitation. A seismic isolator is constituted typically by a package of several rubber pads 1–2 cm thick vertically interspersed with either steel laminas or FRP dry textiles suitably treated. In this latter case the isolator is called FREI (Fiber Reinforced Elastomeric Isolator). FREIs exhibit light weight, easy installation and low cost. In this study, recycled rubber in the form of reactivated EPDM has been used to produce very low cost FREIs, combined with glass fiber reinforcement. To be ready for structural application, the rubber used must be vulcanized correctly to properly create the polymer crosslinking. However, all rubber mechanical properties are strongly affected by curing temperature and curing time. Here, the mechanical properties of a typology of FREI conceived and produced by the authors in prototypes are evaluated through a series of experimental tests and numerical computations, taking into account the different levels of vulcanization degree. Shore A hardness test, uniaxial tensile test, and relaxation test have been conducted and verified through Finite Element (FE) modeling. All collected data allow to precisely determine the curing time and temperature to use in the industrial production to obtain optimal output mechanical properties for FREIs.

1. Introduction

Base isolation is widely used for seismic protection of new and existing structures in medium to high seismicity zones. The isolation devices, which are typically interposed between foundation and superstructure, shift the fundamental frequency of the structure to the range of the seismic spectrum where spectral accelerations are low, thus reducing considerably displacements and accelerations registered on the structural elements belonging to the superstructure [1–3].

Many alternatives have been studied in recent years with the aim of developing low-cost isolation devices [4–15]; nowadays one of the most promising one is the utilization of Fiber Reinforced Elastomeric Isolators (FREIs). A FREI is a package constituted typically by several rubber pads 1–2 cm thick vertically interspersed with FRP dry textiles suitably treated. For example, in Refs. [16,17] fiber glass has been employed. FREIs can be used in several ways: bonded [15,18,19], unbonded [13,16,20], partially bonded [21] and with friction [11], i.e. where there is no bonding between rubber pads and fiber layers. FREIs could be simply installed between the upper structure and the foundation without any bonding or fastening in the so called unbonded application, reducing costs. On the contrary, some other commercial isolators such as High Dumping Rubber Bearings (HDRBs) would cost significantly more, due to the need of using steel laminas instead of FRP, thick steel plates for the supports and lead cores.

Several experimental works have been published on unbonded FREIs (UFREIs) revealing their advantages. First of all, the effective horizontal stiffness of UFREIs is considerably lower when compared with that of the bonded devices, decreasing the seismic force demands [17,22]. This feature is a consequence of the so-called rollover effect which is a sort of quasi-rigid rotation occurring at large deformation under strong earthquakes; such "softening" effect is due to lack of bonding. Another important feature of UFREI is the hardening which occurs at very large deformation. Hardening is a consequence of the late contact between isolator vertical edges and supports. It plays an important role in

* Corresponding author.
E-mail address: gabriele.milani@polimi.it (G. Milani).

https://doi.org/10.1016/j.polymertesting.2022.107496
Received 1 August 2021; Received in revised form 15 December 2021; Accepted 30 January 2022
Available online 31 January 2022

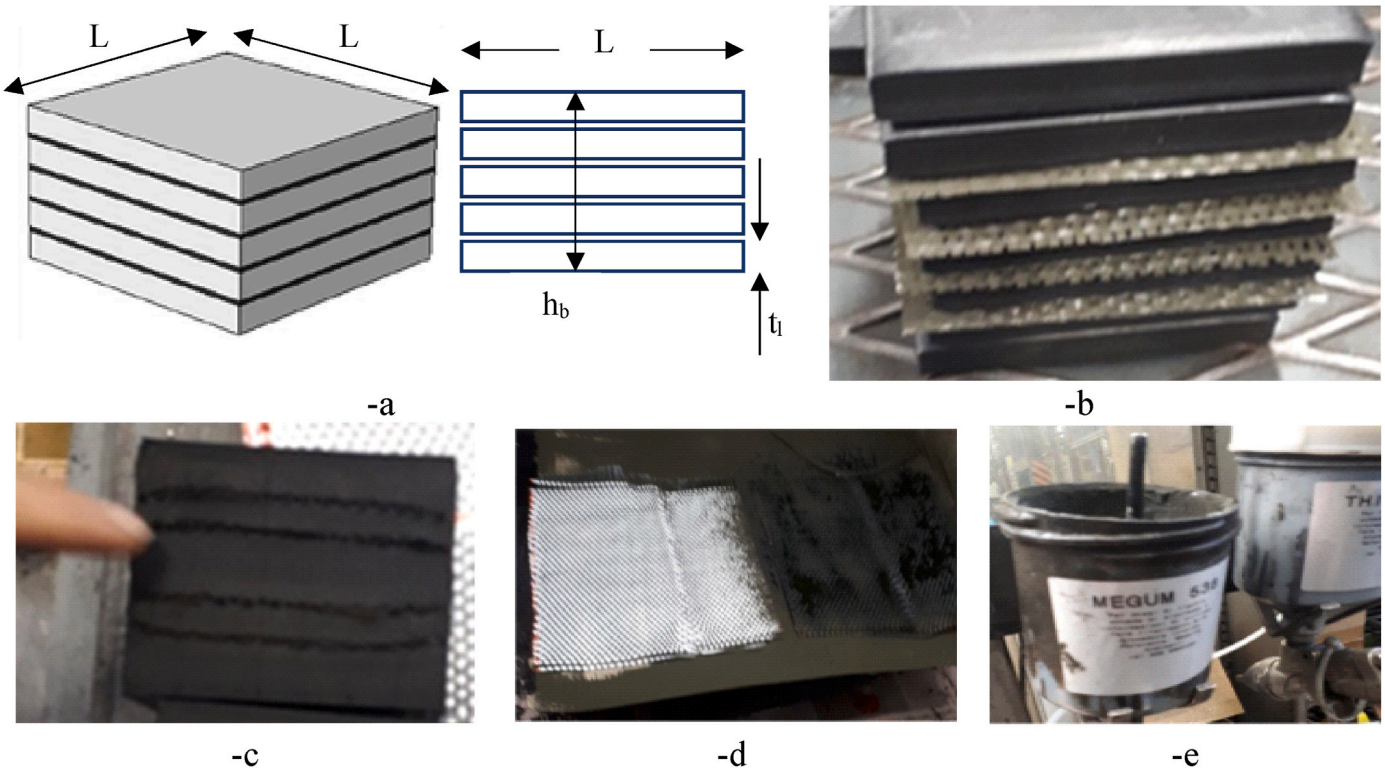

Fig. 1. UFREI isolator production. -a: geometry. -b: assemblage of rubber pads and GFRP dry fabric immediately before vulcanization. -c: middle plane vertical section of the vulcanized item. -d: untreated (white) and treated (black) GFRP fabric. -e: Megum 538 used in combination with Thixon for adhesive bonding between GFRP and rubber.

limiting the shear displacement during a severe seismic event [23,24].

From a chemical point of view, it is paramount that the rubber used for assembling the devices is cured correctly; in particular it is crucial to determine the optimal curing times and temperatures, in order to properly create the polymer network and to make the rubber capable to exhibit good mechanical properties at large strains applied. As a matter of fact, all rubber mechanical properties are strongly affected by curing temperature and curing time. For instance, if a sample is overcured and rubber exhibits reversion (a problem crucial for natural rubber NR), transversal crosslinks break with a consequent macroscopic drop of the device strength.

In this study, a particular FREI prototype conceived by the authors in Refs. [5,13] for low-cost seismic isolation of low-rise masonry buildings is considered. It relies into 5 pads made by regenerated EPDM rubber blends and 4 GFRP dry textiles, treated on the surface with a commercial adhesive to enhance the bond strength at the interface with rubber. First, the rubber material has been studied from a curing and mechanical point of view experimentally. The curing characterization relied into the determination of the optimal vulcanization conditions in terms of time and temperature, a task experimentally accomplished putting rubber into a rheometer chamber and deriving the corresponding rheometer curves at four different temperatures, namely 150, 160, 170 and 180°C. Vulcanization has been conducted with sulfur and accelerants. The mechanical characterization has been carried out performing stress-strain and relaxation tests. In a previous investigation by the authors [5,13] four batches were considered to select the most suitable one to use for the production of low cost isolators; they were obtained blending two virgin commercial rubbers (Vistalon 3666 for Batches 1 and 2 or Dutral 4038 for Batches 3 and 4) with two regenerated EPDMs produced by two different suppliers (named A and B). For instance, in agreement with the aforementioned nomenclature, the label "Batch 2B" referred to Vistalon 3666 blended with regenerated EPDM from B supplier. Among the four batches, it was found that the best performance in terms of vulcanization and final mechanical properties (before and after ageing) was exhibited by Batch 4B, which has been consequently used in the production of the isolator prototypes and which is here considered. Even though rheometer curves indicated that the best vulcanization conditions for the rubber would have been at 150 °C for 40 minutes [25], prototypes were physically produced by a third part factory that provides items at a curing temperature equal to 130 °C. The utilization of a suboptimal temperature has evident consequences on the final properties of the isolator; it has been found an experimental Shore A in the core of the item sensibly lower than that expected. The present research is aimed at showing how a reasoned advanced numerical modeling can predict some critical issues in the vulcanization of thick items, namely in this case the insufficient level of vulcanization obtained in the core of the prototypes, consequence of the too low vulcanization temperature. Different numerical analyses have been carried out discretizing the isolator into Finite Differences (FDs) or Finite Elements (FEs) and deriving the final crosslinking degree, simulating the heating process in an electric oven through 3D elements obeying a Fourier's heat transmission equation. By assuming a first order kinetic law for rubber -suitable for EPDM because reversion is not visible-it has been possible to easily derive the local crosslinking degree. By fitting experimental stress-strain curves and relaxation curves respectively with a Yeoh and viscoelastic Maxwell model (Prony series), it has been then possible to simulate into FEs a standard Shore A durometer test and subsequently compare the numerically obtained Shore A with the experimental one.

Very good agreement has been found between experimental data and numerical predictions, demonstrating that (i) few experimentations are needed to deduce the real mechanical behavior of rubber constituting the pads of an isolator and (ii) the present prototype needs to be vulcanized at 150 °C to avoid the risk of obtaining items under performant. Apart the specific case here analyzed, the procedure proposed may be regarded as general to have an insight into the expected actual mechanical behavior of a rubber isolator limiting the experimentation to

Table 1
Composition of commercial EPDMs Vistalon 3666 and Dutral 4038 and of the four rubber batches obtained with new commercial EPDMs and regenerated rubber.

Vistalon 3666		Dutral 4038	
Product	Phr	Product	Phr
Vistalon 3666	175	Dutral 4038	100
FEF N550 (Carbon Black)	80	FEF N550 (Carbon Black)	70
Sillitin Z (Silica)	80	ZnO (Zinc oxide)	5
Flexon 876 (Paraffinic oil)	120	Stearic Acid	1
ZnO (Zinc Oxide)	5	SRF (Carbon Black)	40
Sillitin Z (corpuscular silica)	0.5	Paraffinic Oil	80
MBT	1.5	Rodrtax 2 (zinc stearate)	4.5
TMTDS	0.8	ZDBDC	1
ZDEDC	0.8	S	2
DTDM	2		

Batch 1A		Batch 2B		Batch 3A		Batch 4B	
Ingredient	gr	Ingredient	gr	Ingredient	gr	Ingredient	gr
EPDM Vistalon 3666 OG	175.00	EPDM Vistalon 3666 OG	175.00	EPDM Dutral 4038 NCS	100.00	EPDM Dutral 4038 NCS	100.00
EPDM Regenerated A	300.00	EPDM Regenerated B	300.00	EPDM Regenerated A	300.00	EPDM Regenerated B	300.00
ZnO Zinc Oxide	9.52	ZnO Zinc Oxide	9.52				
Stearic acid	1.52	Stearic acid	1.52				
PEG 4000	4.00	PEG 4000	4.00	ZnO Zinc Oxide	4.00	ZnO Zinc Oxide	4.00
Polyethylene low molecular weight	5.00	Polyethylene low molecular weight	5.00	Stearic acid	1.00	Stearic acid	1.00
Sillitin N 85	68.00	Stllitin N 85	68.00				
Calcium carbonate	100.00	Calcium carbonate	100.00	Calcium carbonate	40.00	Calcium carbonate	40.00
N550 FEF II (Carbon Black)	72.80	N550 FEF II (Carbon Black)	72.80	N550 FEF II (Carbon Black)	185.00	N550 FEF II (Carbon Black)	185.00
Paraffinic Oil	142.00	Paraffinic Oil	142.00	Paraffinic Oil	95.00	Paraffinic Oil	95.00
MBT Premix	1.92	MBT Premix	1.92				
ZDBC Premix	1.92	ZDBC Premix	1.92				
TDEC Premix	0.80	TDEC Premix	0.80	MBT Premix	1.50	MBT Premix	1.50
TMTD Premix	1.12	TMTD Premix	1.12	Sulfur Premix	2.50	Sulfur Premix	2.50
DPTT Premix	1.12	DPTT Premix	1.12	TMTD Premix	2.00	TMTD Premix	2.00
Sulfur Premix	3.80	Sulfur Premix X	3.80				

DPTT = dipentamethylene thiuram tetrasulfide, DTDM = 4,4'-di-thio-di-morpholine-sulphur, EG 4000 = Polyethylene glycol, Flexon 876 = oil for EPDM extension (EASTM D 2226), MBT = 2-mercaptobenzothiazole, N550 FEF = Carbon black N 550, TMTDS = tetra-methyl-thiuram- di-sulfide, PEG 4000 = Polyethylene glycol, SILLITIN N 85 = silica and lamellar kaolinite, SRF C.B. = thioformaldehyde, TDEC = tellurium diethyl dithiocarbamate, TMTD(S) = tetramethyl thiuram disulfide, ZDB(D)C = Zinc dibutyl (di)thiocarbamate , ZDEDC = di-ethyl di- thiocrbamate.

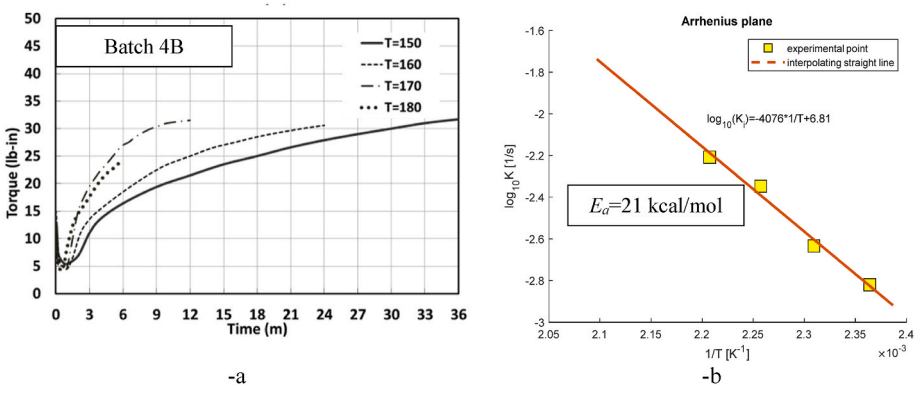

-a -b

Fig. 2. a: Rheometer curves obtained in a previous experimental campaign in specimens made with virgin and regenerated rubber [5]. -b: Experimental determination by linear best fitting of the reaction kinetic constant for the rubber blend.

the strict necessary.

2. Geometry of the isolator studied and materials adopted

The isolator under investigation, specifically conceived by the authors for the installation at the base of low rise masonry buildings in developing countries without any bond, see Fig. 1, has a square cross section equal to 75 × 75 mm (LxL), a height equal to 52 mm (h_b) and is constituted by 5 rubber pads 10 mm thick (t_l), interspersed by a dry GFRP fabric.

The main goal to achieve was the production of low-cost devices exhibiting at the same time a satisfactory mechanical performance, especially under aged conditions. Even though several codes of practice require the substitution of the devices every 10 years, such isolator was indeed conceived with the same service life of common residential buildings (50 years). To cope with such requirements, the expensive head and foot thick steel plates typically used in bonded configurations were removed, GFRP was used instead of steel laminas and EPDM was adopted for the pads instead of Natural Rubber NR. EPDM is indeed much more resistant to ageing than NR, having however a quite low damping, an issue that the authors are still studying, for instance trying to substitute EPDM with blends containing Butyl Rubber IIR. To further reduce costs, instead of using virgin EPDM, authors tested the performance of different pads constituted by a blend of virgin EPDM and

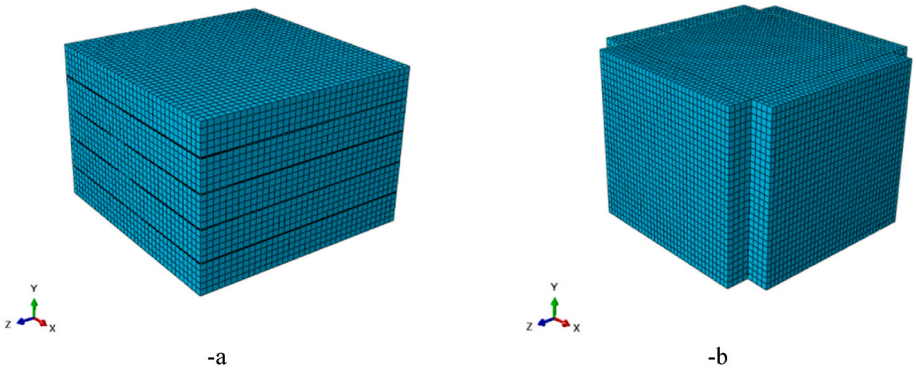

Fig. 3. a: Finite Difference (Matlab) and Finite Element model (ABAQUS) of the FREI prototype without mold meshed. -b: FE model (ABAQUS) of the FREI prototype with mold meshed.

Table 2
Thermal properties of materials.

Property/Material	GFRP	EPDM
Specific Heat Capacity [J/KgK]	850	1200
Heat Conductivity [W/mm°C]	$6.5{\cdot}10^{-5}$	$2.6{\cdot}10^{-4}$

regenerated rubber. In order to have a clear insight into the most suitable formulation to use, during the calibration of the mechanical properties to use for the rubber pads, several attempts were made, with the aim of finding a blend with good hardness and ageing resistance, but at the same time limiting the production costs. In a previous preliminary investigation by the authors [5], four rubber batches were analyzed, consisting of blends with two commercial typologies of commercial EPDMs (Vistalon 3660 and Dutral 4038) and two different regenerated EPDMs provided by two different producers. The composition in phr of the two aforementioned virgin rubbers is summarized in Table 1. As it can be noticed, for Vistalon 3666 paraffinic oil content was quite high and equal to 42% wt; the molecular weight distribution was medium/-large, ENB content was equal to 4.5% and propylene content in weight was 30%. Such characteristics led to obtain after vulcanization soft blends with hardness 30 ± 5 ShA. Mooney viscosities (1 + 4) at 100 °C and 121 °C were respectively equal to 71 and 53. Dutral 4038 contained much less oil and it exhibited a narrow/medium molecular weight distribution, the ENB content was 4.1% and the propylene content 29%. Such characteristics led to obtain after vulcanization relatively hard blends with Shore A equal to 60 ± 5 ShA.

Sulfur was used to crosslink rubber instead of peroxides, again in order to reduce costs to a great extent. Indeed, peroxide vulcanization is very sensitive to humidity and particular equipment is needed, with the subsequence growth of the production costs.

The recipes of the four different batches considered in Ref. [5] are summarized in Table 1.

Batches 1 and 2 were obtained adopting Vistalon 3660 as virgin rubber, whereas batches 3 and 4 were obtained using Dutral 4038. As far as regenerated EPDM is concerned, as already pointed out it was used to partially replace virgin rubbers and limit further production costs. Two different regenerated EPDMs were used, hereafter labeled as A and B, bought by two providers, the first selling recycled EPDM from whether strips in Russia (A), the second in EU (B). Batches 1 and 3 contained A regenerated rubber, whereas batches 2 and 4 contained B regenerated rubber. No precise technical sheets were obviously available for such kind of regenerated materials. However, authors experienced a quite satisfactory reaction capacity during curing for both A and B materials. Furthermore, analyzing Table 1, it is interesting to point out how the amount of carbon black remained essentially unchanged when compared with common virgin EPDM. Such feature suggests that regenerated rubber has a good capacity of crosslinking and cannot be regarded exclusively as a filler surrogate. This is not surprising, because the process of regeneration relies into the partial or almost total devulcanization of the rubber waste and it is well known that devulcanized rubber exhibits a slightly lower crosslinking capability than virgin rubber.

From the comprehensive mechanical characterization made by the authors in Ref. [5] before and after ageing for the different batches (the interested reader is referred there for further details) authors concluded that the most suitable blend to utilize in the industrial production of the

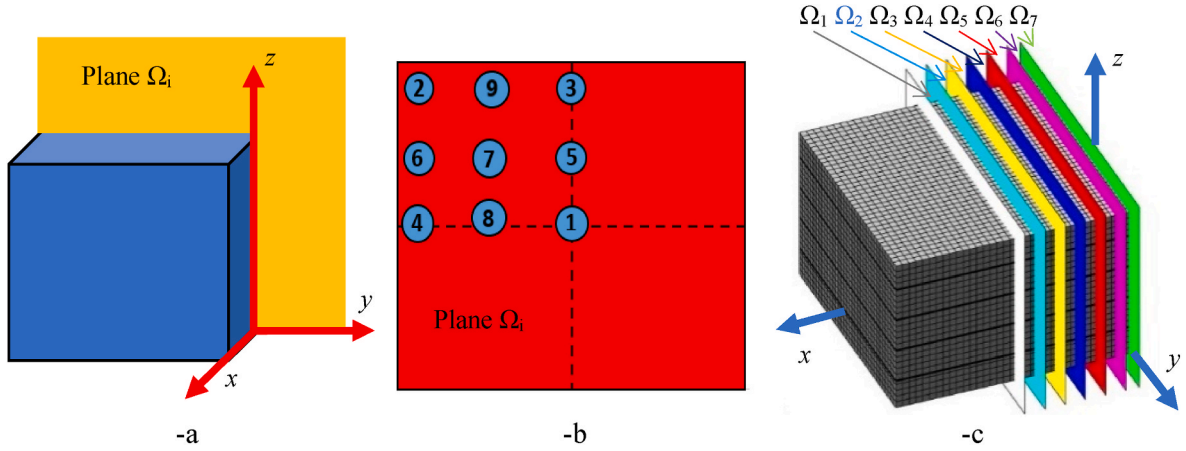

Fig. 4. Reference points and transversal planes considered for computing the temperature profile and the curing level. -a: generic transversal plane Ω_i. -b: points where temperature profile and curing level were checked on a transversal plane Ω_i. -c: transversal planes Ω_i, i = 1, …,7.

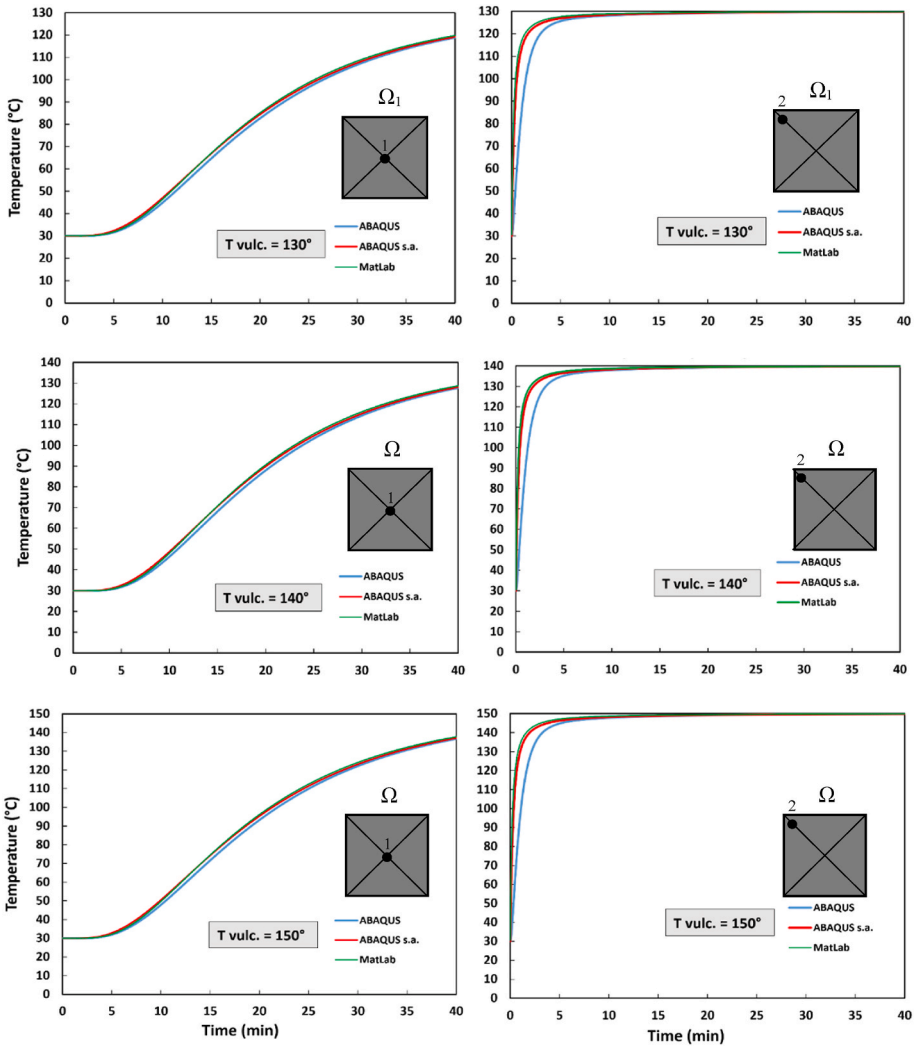

Fig. 5. Comparison between temperature profiles at reference points of the isolator cross section obtained with ABAQUS and with Matlab, at different curing temperatures (curing time equal to 40 min).

aforementioned low cost seismic device is Batch 4B. Among the others, indeed, it exhibits the best ageing behavior, as well as promising overall mechanical properties (e.g. stretch-strain behavior and relaxation) compatible for its utilization for the isolation of low and even medium rise masonry residential buildings. The production of the isolators was therefore carried out using exclusively Batch 4B, which is the only batch considered in the present study.

3. Crosslinking of fiber reinforced elastomeric isolators

In order to be ready for structural applications, rubber needs to be processed through several stages [26]: one of the most important and critical is curing. In such phase, rubber is heated with either peroxides or sulfur, accelerators and activators at around 140–160 °C. Peroxide curing would be preferable because the crosslinking between contiguous chains is obtained on C–C belonging to the backbone. It is therefore more stable, the link exhibiting a much higher energetic content than that associated to S–S. However, the cost of a sulfur vulcanization is sensibly lower and therefore preferable for the production of low-cost devices. Whatever the vulcanizing agent present in the blend is, curing may be defined as the chemical process that triggers the formation of transversal cross-links between long rubber molecules creating the so-called polymer network. Thanks to crosslinking, the chains are prevented from sliding along each other and the rubber becomes elastic, i.e. vulcanizes.

It has been widely shown that the final mechanical properties of rubber (such as elastic modulus, tensile strength, elongation at break, etc) are strongly affected by the degree of curing. In particular, curing temperature and exposition time are critical parameters to establish in order to obtain optimal and homogenously distributed mechanical properties of rubber items [27]. The FREIs considered in this study have been assembled in a previous experimental campaign using regenerated EPDM and commercial virgin rubber (Dutral 4038).

Sulfur curing kinetic is particularly simple for EPDM. Contrarily to NR [28–32], indeed, EPDM does not exhibit perceivable reversion [5,33], even at high vulcanization temperatures. In absence of reversion, a first order kinetic law can be adopted without committing unacceptable errors. Such a feature is confirmed also in the present study, where a blend made with virgin and regenerated rubber is studied. Experimental rheometer curves obtained at four different temperatures (from 150 °C to 180 °C) [5]show that reversion is absent, see Fig. 2, and therefore the following kinetic scheme holds:

$$P \xrightarrow{K(T)} P^* \tag{1}$$

where P and P^* are respectively the uncured and the cured polymer, whereas $K(T)$ is the kinetic constant, function of the temperature T ruling the reaction.

The crosslinking degree α_R, ranging from 0 (unvulcanized rubber) to

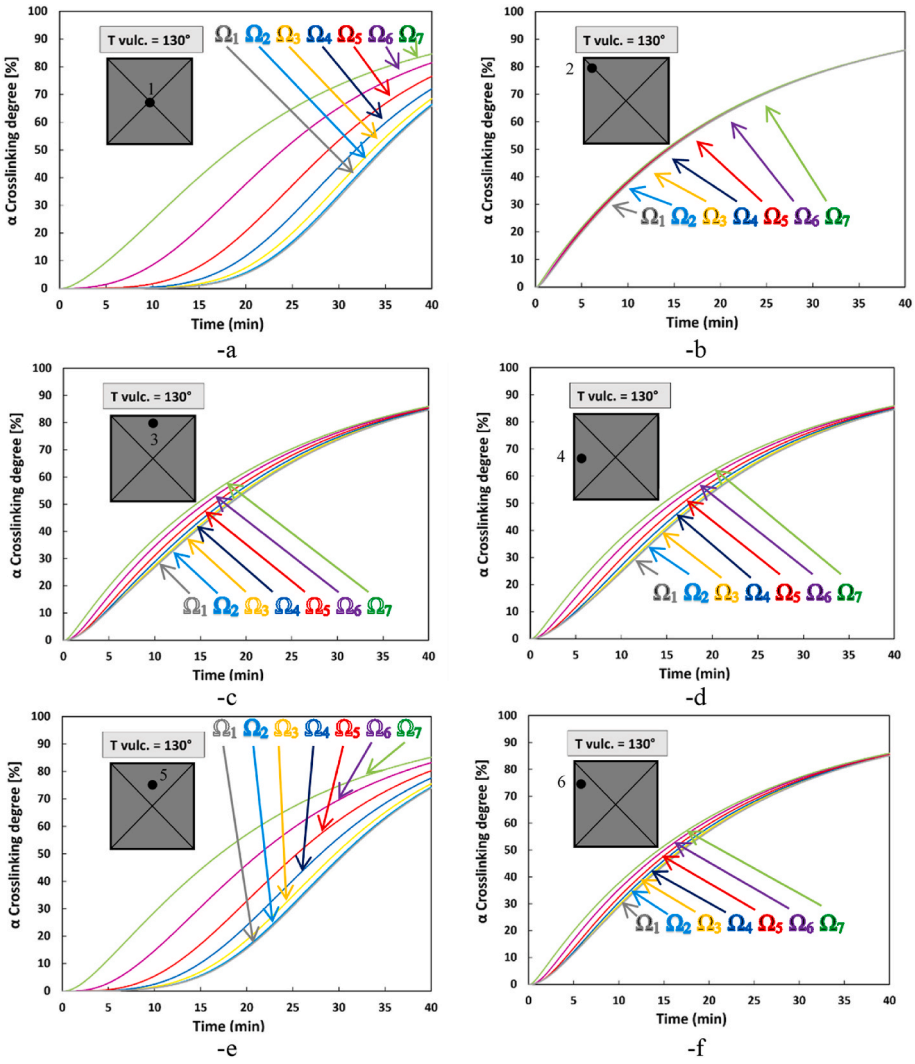

Fig. 6. Crosslinking degree evolution in case of curing temperature equal to 130 °C at reference points 1–6 in all the considered sections of the FREI. -a: P1. -b: P2. -c: P3. -d: P4. -e: P5. -f: P6.

1 (maximum vulcanization) is therefore expressed by the following formula:

$$\alpha_R = 1 - e^{-K(T)t} \tag{2}$$

$K(T)$ is traditionally assumed obeying an Arrhenius law, i.e. its logarithm is linked to the inverse of the absolute temperature by a linear relationship, as follows:

$$\log K(T) = \log K_{max} - \frac{E_a}{R_g}\frac{1}{T} \tag{3}$$

where K_{max} is the kinetic constant at an infinite temperature T, E_a is the activation energy and R_g the universal gas constant. After normalization of the rheometer curve obtained experimentally, see Fig. 2-a, the parameters $\log K_{max}$ and $-\frac{E_a}{R_g}$ can be evaluated by linear interpolation of the data in Fig. 2-b. The procedure allows to predict the degree of vulcanization α_R in each point of the isolator once the temperature profile during curing is known, for instance solving a heat transmission problem resorting to numerical methods (either finite differences or finite elements). Indeed, combining Eqs. (2) and (3) it is possible to deduce the evolution of α_R upon time as follows:

$$\alpha_R = 1 - e^{-10^{\left(\log K_{max} - \frac{E_a}{R_g}\frac{1}{T(t)}\right)}t} \tag{4}$$

The curing level of the FREIs was evaluated numerically using Matlab (Finite Difference Method) and ABAQUS [34] (Finite Element Method), modeling the actual manufacturing process, where the overall device (i.e. rubber pads and GFRP laminas) was assumed cured inside a steel mold (Fig. 1). The aim is to investigate the curing level distribution inside the device when different curing temperatures (130 °C, 140 °C and 150 °C) are used for 40 minutes of exposition. According to rheometer curves (Fig. 2-a), an optimal vulcanization for the rubber compound was found at 150 °C for 40 min. Such vulcanization guarantees also the perfect adhesion between GFRP and rubber pads.

3.1. Finite difference method. Matlab implementation

When FDs are used to evaluate the temperature profile inside an item, the following forward scheme, Eq. (4), can be used, once that the item is discretized into voxels of dimension Δx, Δy and Δz:

$$T^{p+1}_{n,m,r} = T^{p}_{n,m,r} + \alpha\frac{\Delta t}{\Delta x^2}\left(T^{p}_{n+1,m,r} - 2T^{p}_{m,n,r} + T^{p}_{n-1,m,r}\right) + \alpha\frac{\Delta t}{\Delta y^2}\left(T^{p}_{n,m+1,r} - 2T^{p}_{m,n,r} + T^{p}_{n,m-1,r}\right) + \alpha\frac{\Delta t}{\Delta z^2}\left(T^{p}_{n,m,r+1} - 2T^{p}_{m,n,r} + T^{p}_{n,m,r-1}\right) \tag{5}$$

where m, n and r indicate the (n,m,r) voxel p, Δt the time interval and $\alpha = \frac{K}{\rho c}$ where K is the conductivity, c the heat capacity and ρ the density.

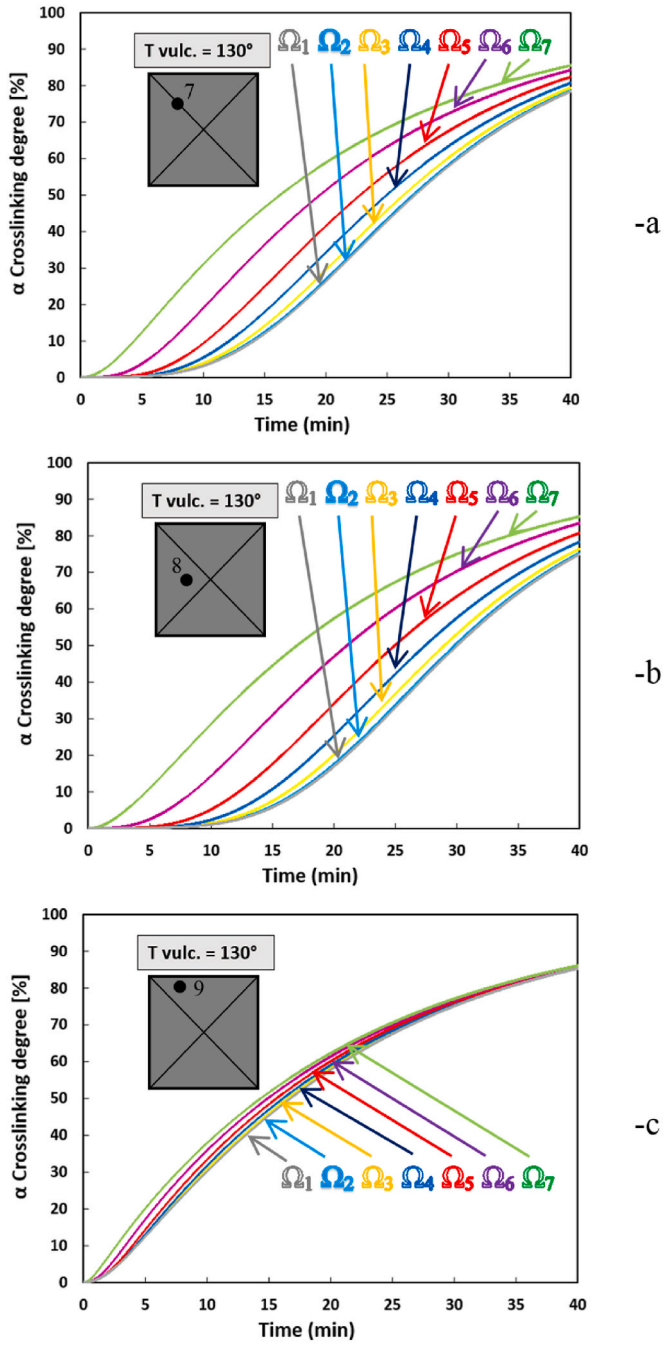

Fig. 7. Crosslinking degree evolution in case of curing temperature equal to 130 °C at reference points 7–9 in all the considered sections of the FREI. -a: P7. -b: P8. -c: P9.

The coefficient of $T^{p}_{n,m,r}$ in Eq. (5) must be positive for thermodynamic consistency. Consequently, the time increment must be constrained as reported in the following Eq. (6):

$$\Delta t < \frac{\Delta x^2 \Delta y^2 \Delta z^2}{2\alpha(\Delta x^2 \Delta y^2 + \Delta x^2 \Delta z^2 + \Delta y^2 \Delta z^2)} \tag{6}$$

In Fig. 3, the discretized isolator considered in the present study is shown. The same mesh used in the FE approach was adopted to make the two numerical procedures mutually consistent. Here, it is only worth mentioning that the finite difference code implemented in Matlab is parametric, i.e. the geometry (e.g. cross section, thickness, number of pads and GFRP reinforcement) can be changed at user's discretion. It has therefore the advantage to provide fast results without the need of remeshing the isolator in case of changes in the geometry. Such feature was particularly appealing in the design phase, because the identification through a trial and error approach of the most suitable temperature and curing time became extremely fast.

3.2. Finite element method. ABAQUS implementation

A 3D geometric model of the isolator was also meshed into FEs using the commercial software ABAQUS, with the aim of assessing the results obtained through FDs in Matlab. Two distinct analyses were performed: (1) a simplified analysis without a mold and (2) an analysis with a steel mold surrounding the FREI (this second case is more representative of the curing process carried out industrially). Both analyses were carried out considering three vulcanization temperatures: 130 °C, 140 °C and 150 °C. A convective heat transfer coefficient equal to $h = 900\ \frac{W}{m^2K}$, suitable to account realistically for the high temperature in the oven, was assumed. In Fig. 3-a, the FE and FD discretization used in the analyses without steel mold is shown. As far as the FE approach is concerned, a total of 53136 linear hexahedral elements of type DC3D8 was used (corresponding to parallelepiped cells in the FD approach, see previous sub-section). The thermal properties assumed for GFRP laminas and EPDM pads are summarized in Table 2.

In order to better represent the curing process adopted in the production phase of the isolator, another analysis considering the steel mold was performed. A steel mold with an equivalent thickness of 10 mm and a heat conductivity of $0.06\ \frac{W}{mm\ °C}$ was directly meshed into FEs, see Fig. 3-b. The faces of the isolators were assumed perfectly bonded to the steel mold using surface to surface tie constraints available in ABAQUS. A total of 78192 linear hexahedral elements of type DC3D8 was used.

3.3. Comparison between FEs (ABAQUS) and FDs

The temperature profiles of two points (one near the corner and one in the core) were monitored in ABAQUS with the aim of comparing the results with those obtained in Matlab, hence assessing the reliability of the FD approach. After such validation, FDs were used in order to quickly predict how the crosslinking degree evolves in the FREI prototype as a function of the exposition time. 9 reference points were monitored along a vertical cross section Ω_i of the isolator, as shown in Fig. 4a-4b. Furthermore, 7 Ω_i transversal cutting planes were considered, ranging from the middle cross section (white plane) to the external vertical face (green plane), see Fig. 4-c.

As already mentioned, two thermal analyses were performed in ABAQUS with and without the steel mold (the latter is reported in the following as ABAQUS simplified analysis - s.a.).

For validation purposes, the temperature profiles obtained at 2 characteristic points belonging to Ω_1 plane (centroid, point 1 and corner of the cross section, point 2) were post-processed to compare FE results with FD ones. Results obtained are shown in Fig. 5, assuming three different temperatures of the oven, respectively equal to 130 °C, 140 °C and 150 °C. As expected, by modelling the steel mold, the related heating of the corner point is slightly delayed. No perceivable differences are visible on the central point, because the heat diffusion requires time for a deep penetration inside the material. As a consequence, point 1 is impacted less by the assumptions made on the boundary conditions.

Generally speaking, it can be affirmed that in Fig. 5 the curves exhibit a good agreement, indicating that the FD code could be effectively used to obtain with satisfactory accuracy the temperature profiles in other points of the cross section.

Having at disposal the temperature profile $T(t)$ of each point of the isolator, using Eq. (4) it is possible to estimate the evolution of the degree of vulcanization point by point. In Fig. 6, the crosslinking degree evolution of points from 1 to 6 (see Fig. 4-b) for all vertical sections Ω_i, i = 1, …,7 is shown when the curing temperature is set equal to 130 °C. Fig. 7 shows the same diagrams for points 7–9. For the FREI cured with a

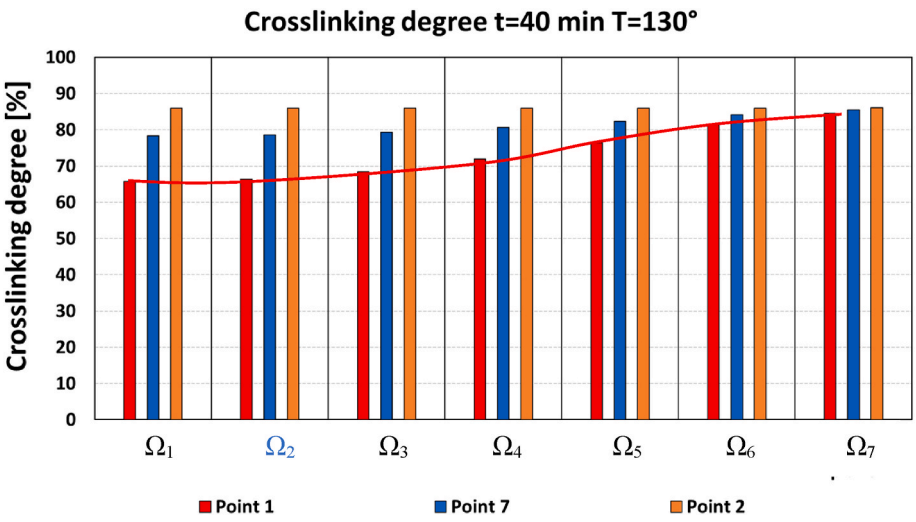

Fig. 8. Crosslinking degree after 40 minutes of curing with a temperature of 130 °C along the diagonal on all the transversal sections of the FREI prototype.

temperature of 130 °C, it is found that the crosslinking degree is certainly insufficient in most of the regions of the device. Moreover, as expected, going from the middle to the external plane, the curing level is not homogeneously distributed. This affects the final local hardness (linked to the curing level) and thus final rubber mechanical properties.

In Fig. 8, the final crosslinking degree (after 40 min) at a curing temperature of 130 °C is shown in bar format for points 1, 2 and 7 (i.e. points along the diagonal of the cross section) belonging to planes Ω_i, i = 1, …,7. It is clearly visible how the curing level decreases passing from external points to inner ones. Considering for instance point 1 (centroid of cross section Ω_i), the crosslinking degree decreases non-linearly (red curve) from 85% near the edge (Ω_7) to 65% in correspondence of the FREI centroid. A similar behavior is observed for point 7, whereas for the external region (point 2) there is no perceivable variation, obviously because such region is located nearby the external boundary. From simulation results, it can be concluded that the curing temperature is certainly suboptimal for all points (<90%), reflecting in particular for internal regions in a critical suboptimality of the vulcanization degree. It would be therefore recommended either to prolong the exposition time or better to increase the oven temperature.

As discussed for a curing temperature equal to 130 °C, the local reticulation evolution was numerically simulated also at 140 °C. In Fig. 9, the crosslinking degree evolution is shown for points from 1 to 6. Fig. 10 shows the same results of Fig. 9 but for points 7, 8 and 9. Unlike the previous case, the vulcanization degree appears generally satisfactory, ranging between 85% and 100% for all points investigated, even for those located in the core of the device. It can be therefore affirmed that a temperature of vulcanization equal to 140 °C leads to a better and more homogeneous crosslinking, with an expected higher homogeneity of the obtained mechanical properties.

The final curing degrees after 40 minutes of exposition for points 1,2 and 7 are collected in the bar plot of Fig. 11. Similarly to the 130 °C case, it is found that passing from the skin to the core there is a drop of the final crosslinking, especially for point 1 that is located deep in the core of the vertical cross section; however and as expected, such drop is much less critical, with a maximum gap between external and internal layers not exceeding 12%. An optimal curing is registered in all points near the external surface, with a curing degree exceeding 90%, even in the most internal section Ω_1.

Finally, the numerical simulations of the heating process were repeated when the oven temperature is set equal to 150 °C. Crosslinking degree evolutions for points 1–6 and 7–9 are depicted respectively in Fig. 12 and Fig. 13. As it is possible to notice, the vulcanization degree obtained at the end of the heating process (40 min) is very high from the skin to the core and almost homogeneous everywhere. Such conclusion is supported by the final crosslinking degree estimation for points 1, 7 and 2, represented in Fig. 14 in bar format. As can be seen and contrarily to the results obtained for an oven temperature equal to 130 °C and 140 °C, the final crosslinking degree is very high everywhere, exceeding abundantly 90%. It is also clearly visible how all points reach a homogeneous value of crosslinking (almost equal to 100%), even in the inner portions.

The sensitivity analysis carried out shows how a vulcanization temperature of 130 °C is totally unsuitable to produce seismic isolators with good mechanical properties, demonstrating once again that the utilization of consolidated rules of thumb in the production process cannot be a sound approach to follow, because it frequently leads to the realization of devices with too large scatter in the final mechanical properties.

4. Mechanical properties

In order to obtain a suboptimal curing level in dumb bell laboratory samples used to characterize rubber pads, taking into account that an optimal vulcanization is obtained by curing the specimens at 170 °C for 10 minutes (which leads to a rubber compound with an expected hardness of 60 Shore A according to Ref. [5]), two families of rubber specimens (Batch 4B) were vulcanized at 170 °C for 2 minutes and 2.5 min, respectively. In the following, the first is labeled as S-"Soft" and the latter as H-"Hard". Subsequently, Shore A hardness was measured on rubber samples with a thickness of 6 mm (obtained overlapping 3 pads 2 mm thick) according to ISO 7619-1 prescriptions [35]; values of 50 Shore A and 53 Shore A were obtained respectively for the samples cured for 2 minutes and for those cured for 2.5 min, confirming that the vulcanization conditions used lead to an under vulcanization of the specimens. Then, stress-strain and relaxation tests were performed on the specimens to characterize the rubber mechanical properties. A previous study presented in Ref. [13] has shown that these two tests capture well respectively the rubber's hyper-elastic and viscous model parameters.

4.1. Experimental shore a hardness

The results obtained in the previous section show that the FREI cured with a temperature of 130 °C for 40 minutes exhibits a non-uniform curing level. Consequently, rubber mechanical properties are not homogenous within the isolator. On the other hand, a curing temperature of 150 °C would have led to a homogenous curing with constant

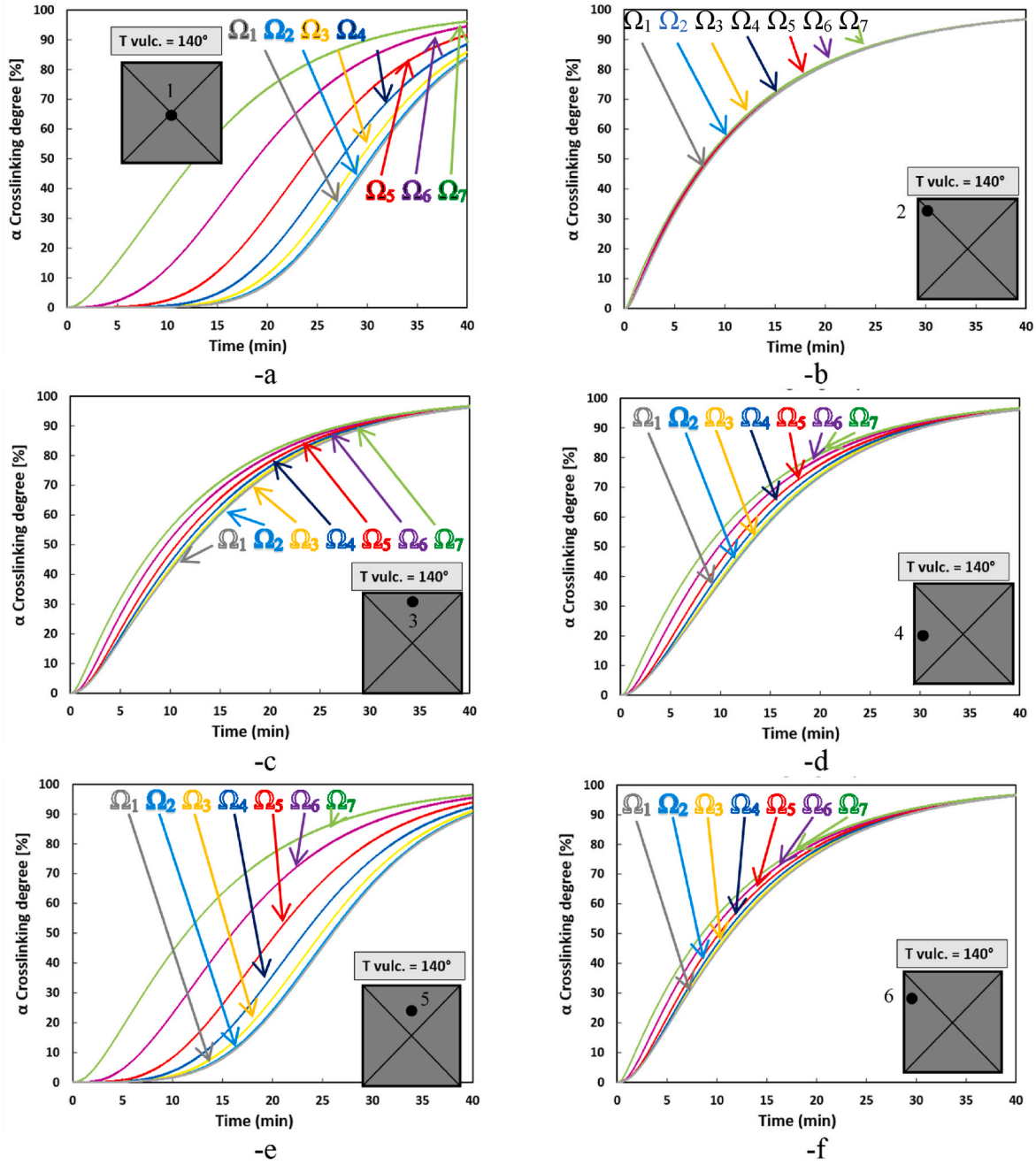

Fig. 9. Crosslinking degree evolution in case of curing temperature equal to 140 °C at reference points 1–6 in all the considered sections of the FREI. -a: P1. -b: P2. -c: P3. -d: P4. -e: P5. -f: P6.

mechanical properties along the thickness.

After two knife cuts on the middle vertical section and along the diagonal, see Fig. 15, of the under-vulcanized device (i.e. cured at 130 °C), Shore A hardness was experimentally measured with a digital Shore A durometer. As expected and as visible in the color map of Fig. 15, hardness varies in Section 1 with a roughly polar symmetry passing from inner to outer points, increasing from 48 ± 2 Shore A in the core to 60 ± 2 Shore A near the skin. An almost identical trend is observed along the diagonal cross section (Section 2).

4.2. Uniaxial tensile tests on S and H specimens

In order to characterize the rubber tensile properties, uniaxial tensile tests based on ISO 37 [36] were performed for both S (i.e. soft, 50 Shore A rubber) and H (i.e. hard, 53 Shore A rubber) specimens. In both cases three samples in the form of dumb bell pieces with an average thickness of 2 mm, see Fig. 16-a, were tested in a uniaxial tensile testing machine, see Fig. 16-b. The specimens were stretched up to failure to define tensile strength and strain at failure, see Fig. 16-c. It is worth noting that the final stress strain curves used in the following to characterize the rubber behavior represent an average of three identical experimental tests.

In Fig. 17, the obtained experimental stress-strain curves are depicted. As visible, S and H specimens show a very similar shape of the curves. The ranges of failure strain and tensile strength for both are about 480–500% and 4.6–5.0 MPa, respectively. Even though the failure strain and tensile strength values are comparable, as expected, the H specimens, which exhibit a higher value of hardness, are slightly stiffer.

The rubber behavior could be modelled using a hyperelastic material based on the definition of the strain energy density function. In agree-

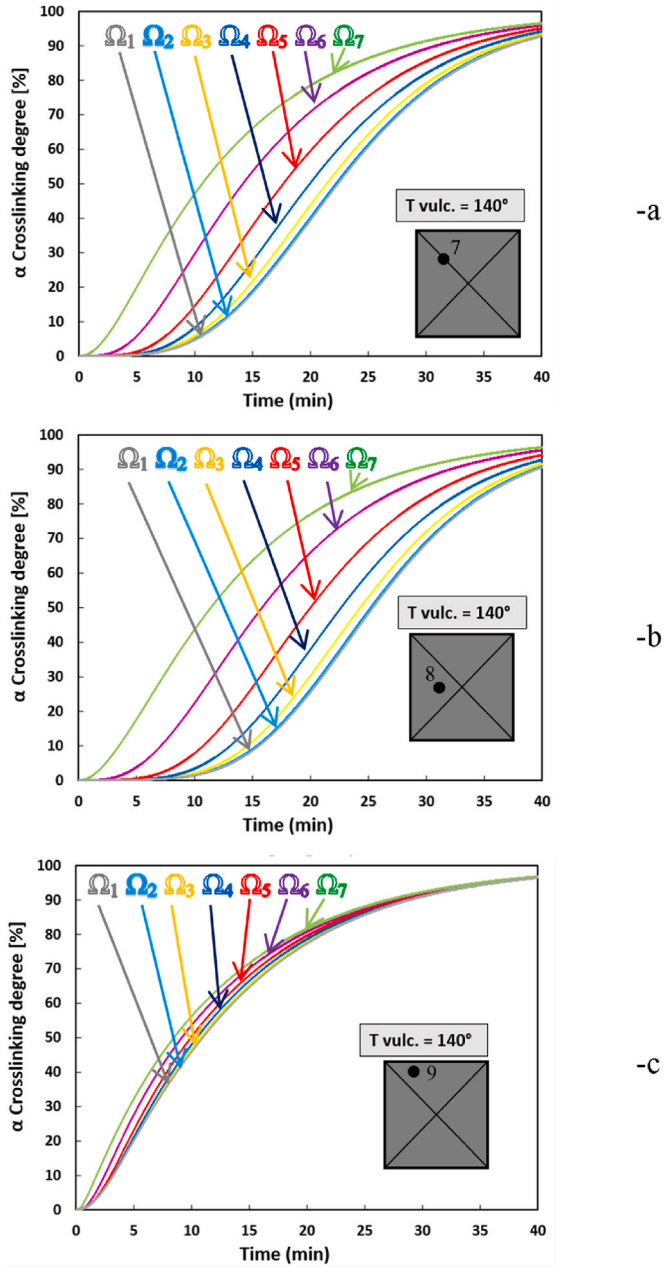

Fig. 10. Crosslinking degree evolution in case of curing temperature equal to 140 °C at reference points 7–9 in all the considered sections of the FREI. -a: P7. -b: P8. -c: P9.

ment with a consolidated experience of the authors in the field, a Yeoh model was used [37]. In such model the strain energy density function W is defined as follows:

$$W = \sum_{i=1}^{3} C_{i0}(I_1 - 3)^i + \sum_{i=1}^{3} \frac{1}{D_1}(J_{el} - 3)^{2i} \tag{7}$$

In Eq. (7) I_1 is the first invariant of left Cauchy-Green deformation tensor, J_{el} is the elastic volume ratio and C_{i0}, D_1 are constants.

In Abaqus, the material coefficients of the Yeoh model were calibrated from the experimental stress-strain data. The material parameters in the FE software code were determined through a least-squares fitting procedure, minimizing the relative stress error. For the n nominal-stress–nominal-strain data pairs, the relative error measure E is typically minimized as follows:

$$\mathrm{E} = \sum_{i=1}^{n} \left(1 - \frac{T_i^{th}}{T_i^{test}}\right)^2 \tag{8a}$$

Where T_i^{test} is a stress value from the test data, and T_i^{th} comes from uniaxial nominal stress expressions, see following Eq. (9). Abaqus minimizes the relative error rather than an absolute error measure since this provides a better fit at lower strains.

The uniaxial deformation mode is characterized in terms of the principal stretches, λ_i, as follows:

$$\lambda_1 = \lambda_U,\ \lambda_2 = \lambda_3 = \frac{1}{\sqrt{\lambda_U}} \tag{8b}$$

where λ_U is the stretch in the loading direction and the nominal strain is defined by $\varepsilon_U = \lambda_U - 1$. To derive the uniaxial nominal stress T_U, ABAQUS invokes the principle of virtual works:

$$\delta U = T_U \delta\lambda_U,$$

so that

$$\mathrm{T}_U = \frac{\partial \mathrm{U}}{\partial \lambda_\mathrm{U}} = 2\left(1 - \lambda_U^{-3}\right)\left(\lambda_U \frac{\partial \mathrm{U}}{\partial \bar{I}_1} + \frac{\partial \mathrm{U}}{\partial \bar{I}_2}\right) \tag{9}$$

In Fig. 18, the experimental stress strain curves are compared with those obtained applying the Yeoh model. As it can be observed, the Yeoh model is perfectly capable to numerically reproduce the actual rubber hyperelasticity [38].

4.3. Relaxation tests on S and H specimens

The viscoelasticity parameters of rubber can be obtained from a relaxation test. During such test, the material is subjected to a sudden imposed strain which is kept constant over time. The stress is then recorded: after the first elastic phase, rubber relaxes due to viscous effects and so the measured stress decreases progressively. The device used for the relaxation test was exactly the same used for the uniaxial tensile test, i.e. an Instron universal testing machine. A target strain of 150% was set. The tests were performed on three identical samples for both S and H specimens. The final curve reported here represents the average of three replicates.

Once the experimental data of the relaxation test were obtained, data were transformed in the form of normalized stresses. In such curves, the initial stress at t = 0 s is the maximum value of the stress registered and is normalized to 1. The relaxation was conducted for 100 s because no remarkable stress reduction was observed after that timeframe.

In Fig. 19, the relaxation test curves and the corresponding normalized stress curves for both compounds are shown. It can be observed that the H specimen (53 shore A) is characterized by a slightly less viscous behavior compared to the S specimen (50 Shore A).

The normalized relaxation curves can be fitted by a Prony [39,40] series, which is based on the viscoelastic generalized Maxwell model. It is a viscoelasticity model available in ABAQUS to model the time-dependent stress strain relationship as expressed in Eq. (10):

$$G(t) = G_\infty + \sum_{k=1}^{K} G_k e^{-\frac{t}{\tau_k}} = G_0 \left[1 - \sum_{k=1}^{K} g_k \left(1 - e^{-\frac{t}{\tau_k}}\right)\right] \tag{10}$$

The rheological model of the stress relaxation function $G(t)$ is shown

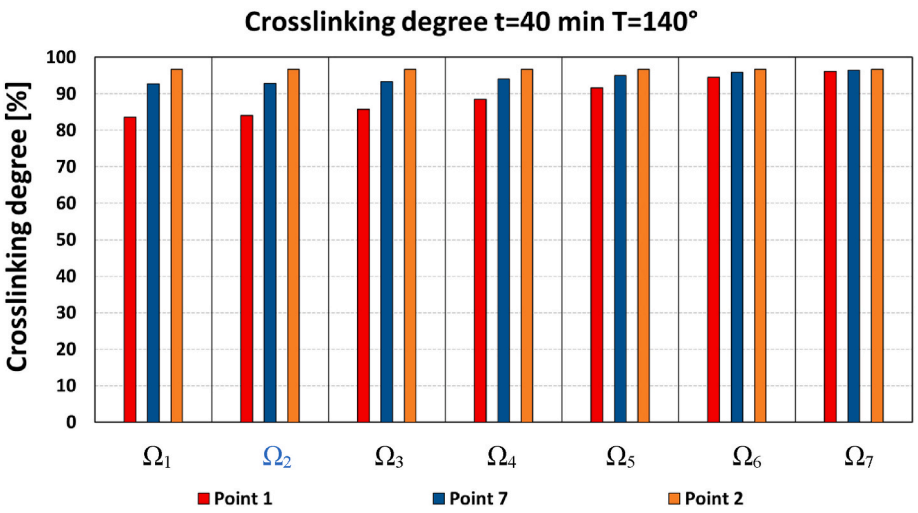

Fig. 11. Crosslinking degree after 40 minutes of curing with a temperature of 140 °C along the diagonal on all the transversal sections of the FREI prototype.

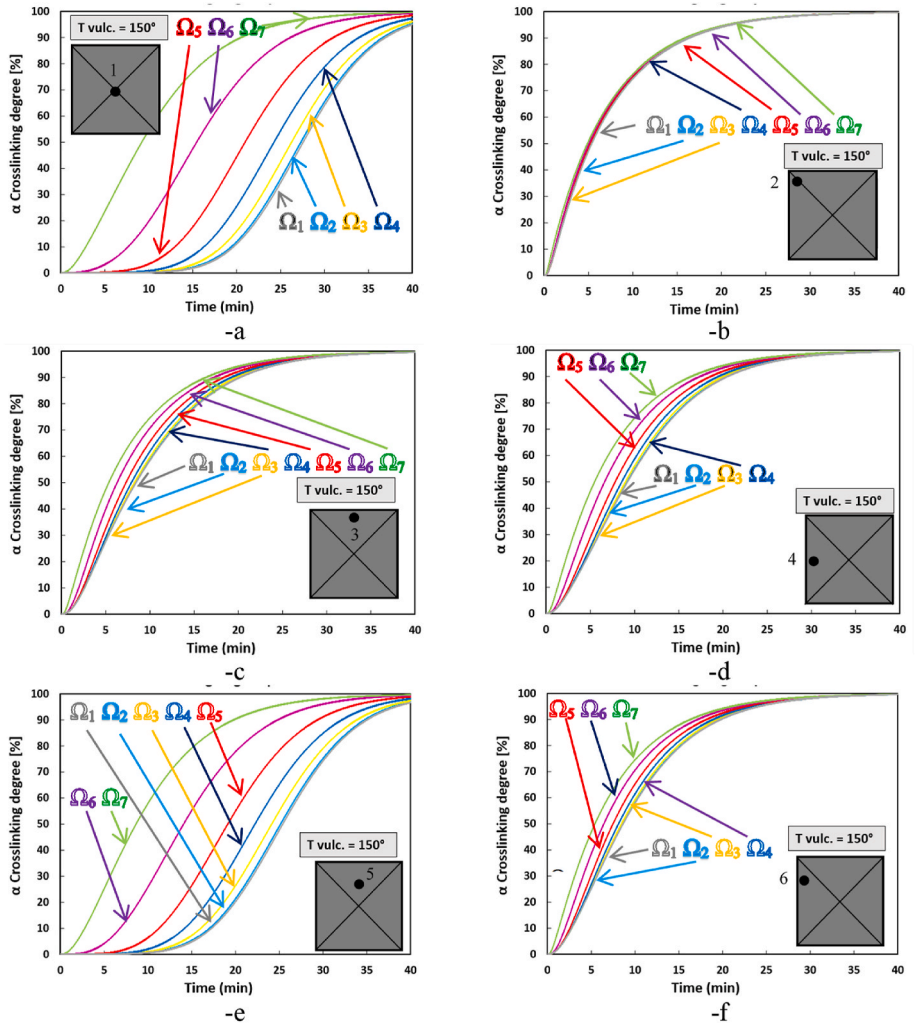

Fig. 12. Crosslinking degree evolution in case of curing temperature equal to 150 °C at reference points 1–6 in all the considered sections of the FREI. -a: P1. -b: P2. -c: P3. -d: P4. -e: P5. -f: P6.

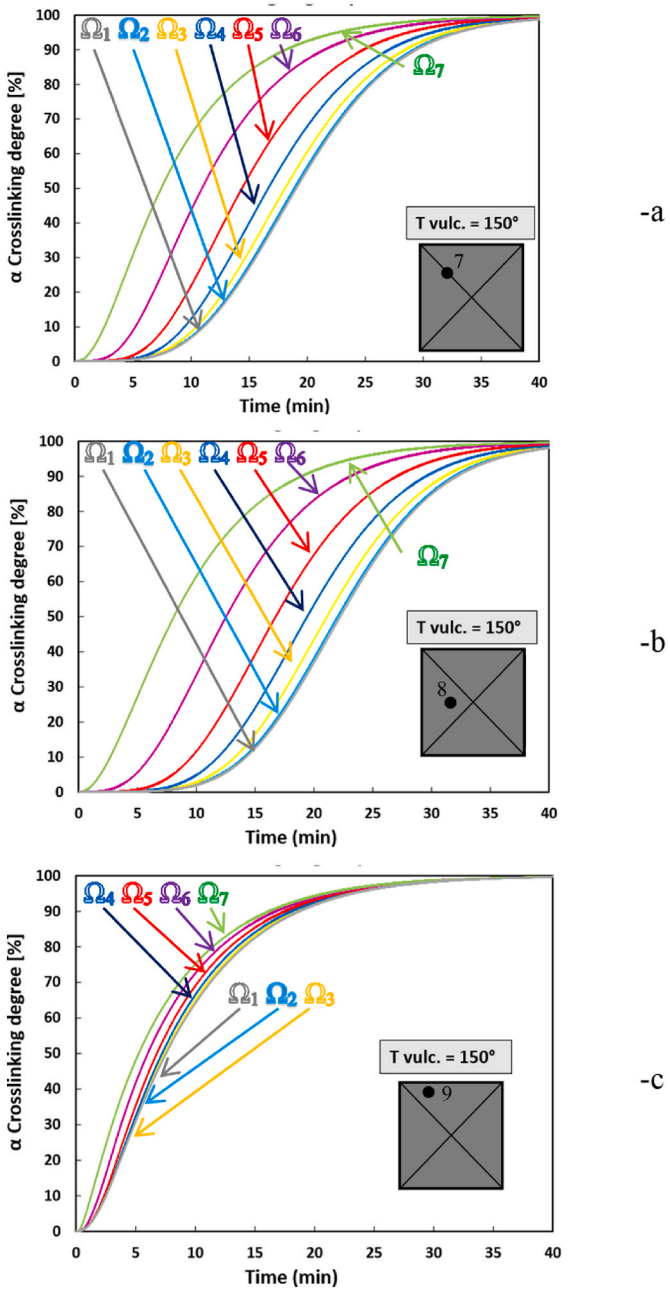

Fig. 13. Crosslinking degree evolution in case of curing temperature equal to 150 °C at reference points 7–9 in all the considered sections of the FREI. -a: P7. -b: P8. -c: P9.

in Fig. 20.

As visible, the model is constituted by nonlinear elastic springs representing the elastic response of rubber and a finite number of Maxwell elements (springs and dashpots) which describes the viscoelastic behavior [41]. In ABAQUS, the right side of Eq. (10) is given in input, where the parameters have the following meaning:

$G_0 = shear\ modulus\ at\ time\ t = 0$

$G_k = dimensionless\ Prony\ coefficient$

$\tau_k = relaxation\ time\ defined\ as\ \dfrac{\eta_k}{G_k}$

Abaqus automatically calculates the Prony series terms when relaxation test data are specified. The normalized shear is defined as:

$$j_S(t) = G_0 J_S(t)$$

Where $J_S(t) = \gamma(t)/\tau_0$ is the shear compliance, $\gamma(t)$ is the total shear strain, and τ_0 is the constant shear stress. At time t = 0, $J_S(0) = 1$.

The relaxation data are converted through the convolution integrals:

$$\int_0^t g_R(s) J_s(t-s) ds = t$$

Abaqus then uses the normalized shear modulus $g_R(t)$ in a nonlinear least-squares fitting to determine the Prony series parameters $(\overline{G}_i^P, \overline{K}_I^P \tau_i^K)$.

Fig. 21 shows a comparison between the normalized experimental relaxation test curve and the Prony model prediction in ABAQUS (subfigure -a refers to S specimens and subfigure -b to H specimens). As visible, two Maxwell elements are sufficient to properly describe the rubber viscoelasticity.

4.4. FE model verification through Shore A hardness test

After the calibration of the hyperelastic and viscous parameters of the material directly in ABAQUS (respectively assuming a Yeoh model and a Prony series), it was possible to simulate with the FE software a standard hardness test.

On a Shore A durometer test, see Fig. 22, the indenter is connected to the outer casing by a spring. During the hardness measurement, the outer casing is moved downwards until it touches the rubber surface (2.5 mm). On the other hand, the indenter moves upward by a quantity which depends on the rubber hardness. Such working mechanism is schematically represented in Fig. 22.

The relationship between the force measured and the movement of the indenter (or of the spring) is expressed by the following equation:

$$F = 0.55 + 3\,\Delta L = 0.55 + 3(L_1 - L_0) \tag{11}$$

In ABAQUS, axisymmetric elements (CAX8H) were used, assuming active a cylindrical sample of rubber sufficiently large (20 times the diameter of the indenter). It is worth noting that -looking at the numerical results-such volume is superabundant, being the rubber volume involved by perceivable deformation much smaller, see Fig. 22. Such outcome a-posteriori confirms that the geometry assumed for the simulations is adequate. Rubber was modelled with a hyperelastic viscous material (Yeoh model + Prony series), with mechanical coefficients set according to the previously discussed tensile and relaxation tests. The steel casing and the indenter were modelled as elastic materials. No friction was considered between rubber, indenter, and outer casing. The spring was modelled using an axial connector between the outer casing and the indenter.

The Shore A hardness was computed from the FE output CU1 (i.e. spring relative displacement in y direction) considering the following relationship:

$$H_a = 40\,x \tag{12}$$

where x is the relative displacement of the indenter.

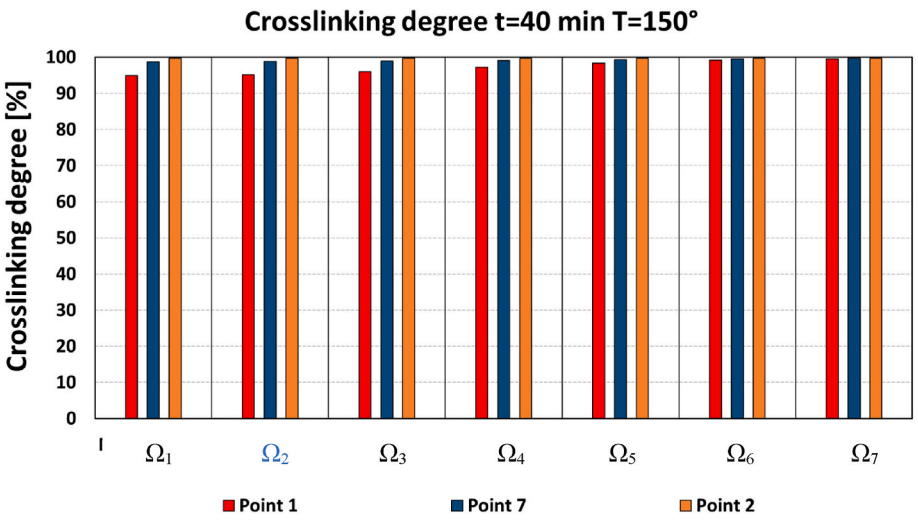

Fig. 14. Crosslinking degree after 40 minutes of curing with a temperature of 150 °C in all the points and along all the transversal sections of the FREI prototype.

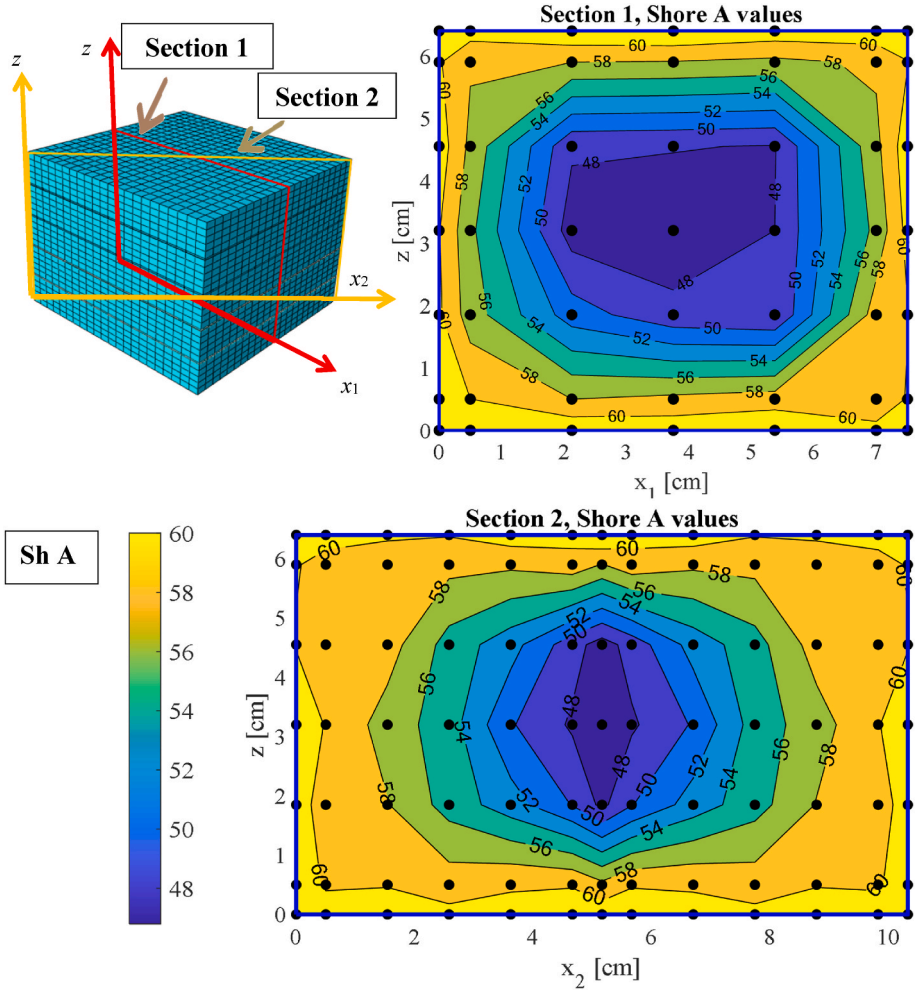

Fig. 15. Shore A hardness measured on the middle vertical section and along the diagonal of a device using rubber specimen S.

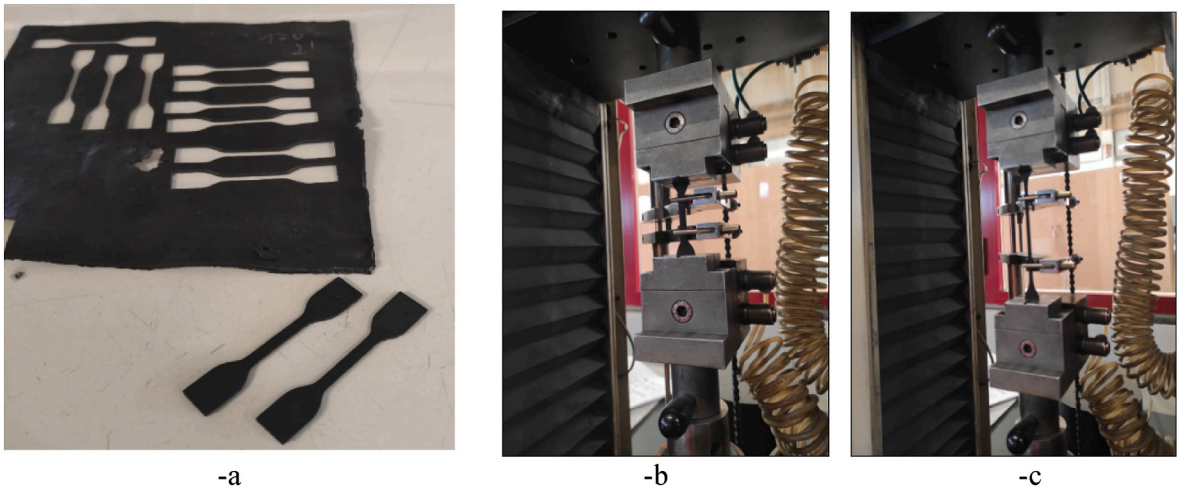

-a -b -c

Fig. 16. (a) Dumb-bell specimens of rubber, (b) the uniaxial tensile test device, (c) stretching of the rubber specimen.

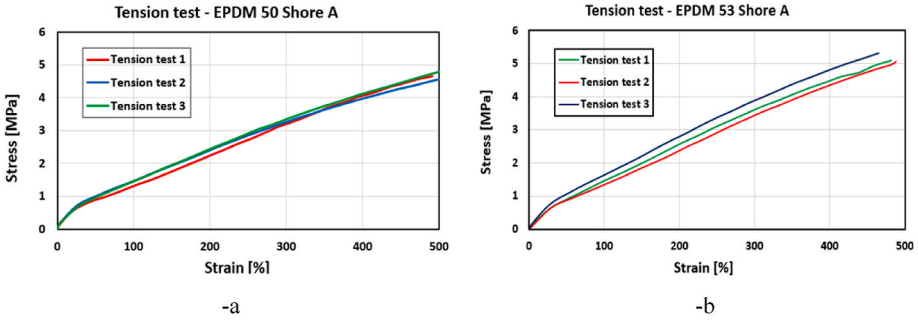

-a -b

Fig. 17. Experimental stress-strain curves for the S specimen (50 Shore A) and H specimen (53 Shore A).

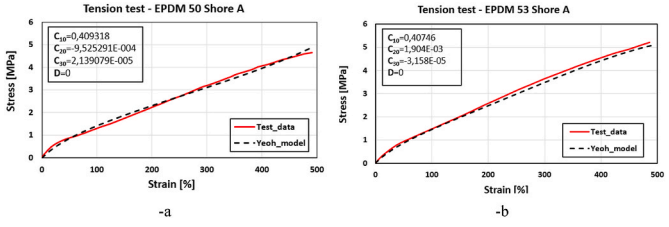

-a -b

Fig. 18. Comparison between experimental data and Yeoh model for the specimens S (-a) and H (-b).

In Fig. 22, the deformed shape of the FE model obtained for the H compound (53 Shore A) is presented. Similar results were obtained for the S compound. In Fig. 23, the hardness evolution upon time for S (subfigure -a) and H (subfigure -b) models is plotted. Obviously, since rubber was modelled with a viscous elastic material, a relaxation of hardness is clearly visible with a stabilization to the target value after about 20 s. In Table 3 the relaxed numerical values of hardness and the relative error with respect to the experimental ones are summarized. As it can be noticed, the hardness computed in ABAQUS is slightly larger than the experimental one. However, the relative errors are lower than 5%, hence fully acceptable from an engineering point of view.

5. Conclusions

The paper presented a combined experimental and numerical approach for the accurate evaluation of the mechanical properties of Fiber Reinforced Elastomeric Isolators (FREIs) made of reactivated EPDM and vulcanized under pre-established conditions. The standard production chain of the low cost FREIs consisted into a curing in the mold for 40 minutes at an oven temperature of 130 °C. Being aware that such temperature is suboptimal, the study carried out was aimed at a better understanding of the influence of crosslinking on the mechanical properties of the bearings.

The crosslinking degree reached locally was numerically evaluated solving a 3D heat exchange problem by means of both Finite Difference (Matlab) and Finite Element (ABAQUS) methods. The results showed that curing the device for 40 minutes at a temperature of 130 °C is responsible for a severe local suboptimal curing, which varies considerably from inner to outer points. On the contrary, numerical predictions showed that curing the isolator at 150 °C for the same timeframe leads to

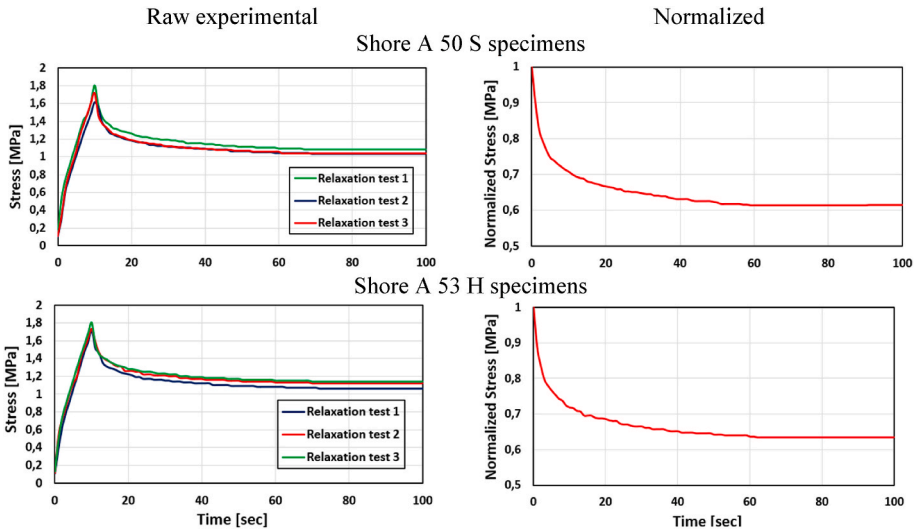

Fig. 19. Relaxation test raw experimental (left) and normalized (right) curves on three samples of specimens S (top subfigures) and H (bottom subfigures).

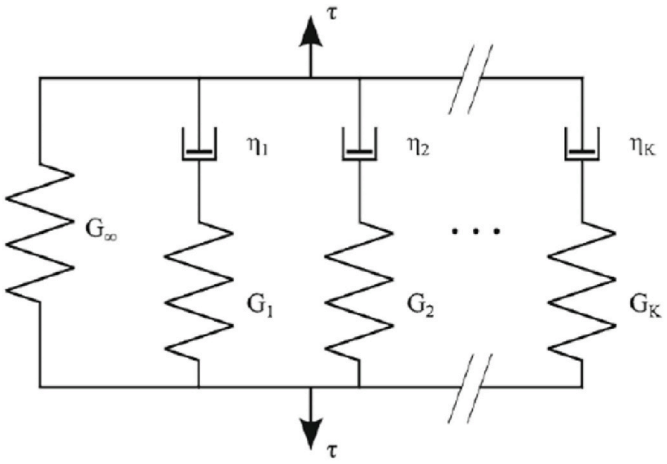

Fig. 20. Rheological (Maxwell) model of the relaxation function G(t) [41].

an optimal and homogenous distribution of the curing level, which exceeded 90% even for the inner points.

After a double knife-cut on the FREI device, Shore A hardness was measured on the middle vertical section and along the diagonal. It was experimentally found a considerable hardness variation from inner to outer points, passing respectively from 48 ± 2 Shore A to 60 ± 2 Shore A. Such experimental evidence confirmed that the mechanical properties were not homogenously distributed within the isolator.

Uniaxial tensile tests and relaxation tests were also performed to obtain the hyperelastic and viscoelastic properties of the rubber pads in case of Shore A equal to 50 (S soft rubber) and 53 (H hard rubber). Such experimentation was crucial to correctly define a 3D FE model that can be used to simulate the cyclic shear behavior of a real isolator. The ranges of failure strain and tensile strength found were about 480–500% and 4.6–5.0 MPa, respectively. Even though the failure strain and tensile strength values were comparable, as expected, H specimens (which exhibited higher value of hardness), were slightly stiffer. The relaxation test result showed that H specimens (53 shore A) provided a slightly less viscous behavior compared to S specimens (50 Shore A). In order to evaluate correctly all the material visco-elastic coefficients, a FE numerical Shore A measurement was performed, confirming the experimental hardness with satisfactory accuracy. Such procedure has also demonstrated that this model can reduce costs and optimize planned outage times. In particular, by means of FE cyclic shear tests, it is possible to evaluate in a preliminary step reliable damping ratio, horizontal stiffness, and shear modulus of the rubber compound without performing more expensive and time-consuming experimental tests [13].

For future research developments, the authors are performing new numerical and experimental tests on the devices. In particular, the first

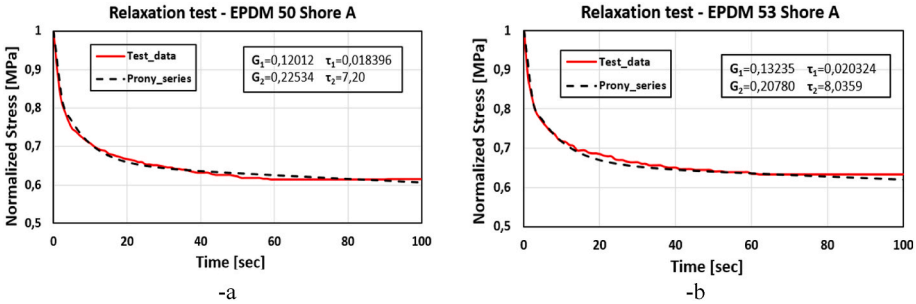

Fig. 21. Comparison between experimental test data and viscoelastic generalized Maxwell model for specimens S 50 Shore A (-a) and H 53 Shore A (-b).

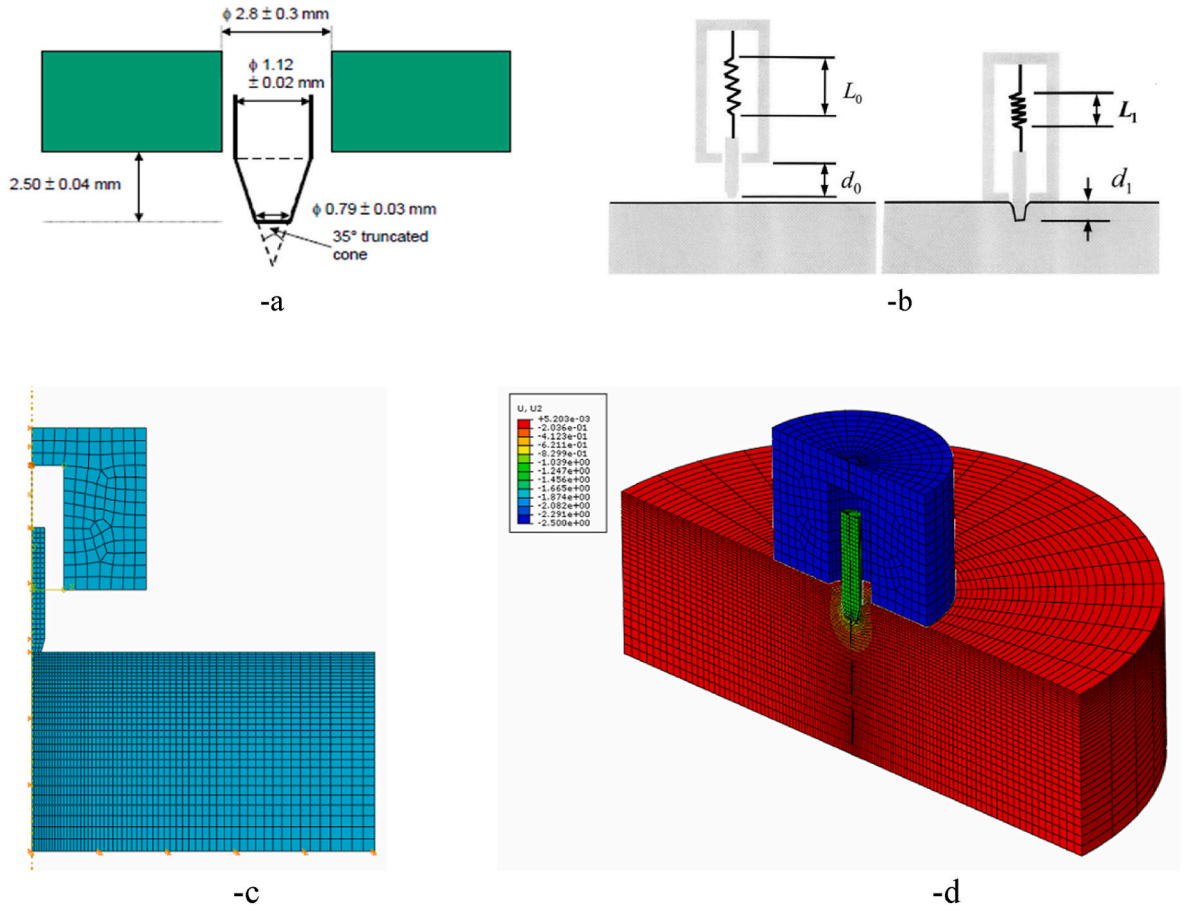

Fig. 22. a: Shore A durometer geometrical features. -b: Schematic representation of the working mechanism. -c: axisymmetric mesh used to simulate the penetrometer test. -d: deformed shape at full penetration of the truncated cone.

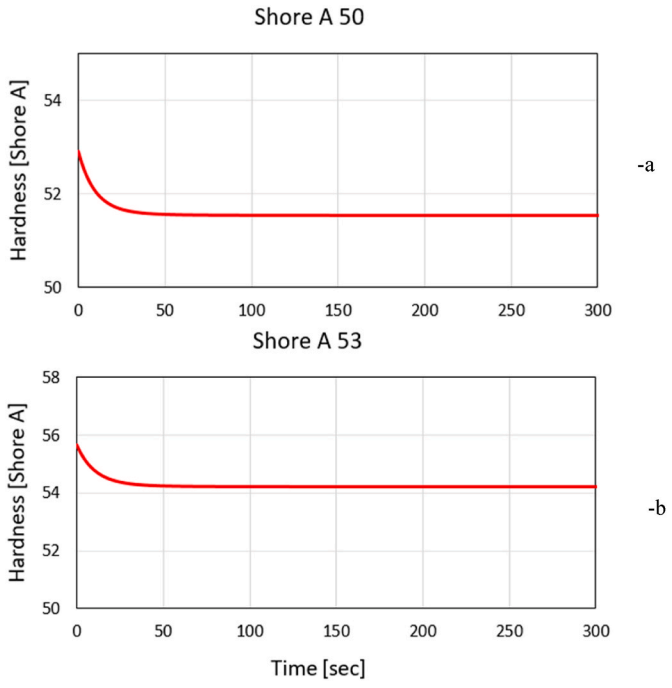

Fig. 23. Evolution of the numerical hardness for specimens S 50 Shore A (-a) and H 53 Shore A (-b).

Table 3
Hardness value for the two rubber compounds.

Rubber specimens	Spring Displacement [mm]	Numerical Hardness Value [Shore A]	Experimental Hardness Value [Shore A]	Error [%]
S	1.2	51.50	50	3
H	1.356	54.24	53	2.28

results obtained with FE cyclic shear tests of the FREIs seem promising for their implementation as base seismic isolators of low-rise masonry buildings in developing counties. Simultaneously different prototypes have been produced, and soon, compression and cyclic shear tests will be performed for a comprehensive seismic characterization.

Declaration of competing interest

The authors declare that they have no known competing financial interests or personal relationships that could have appeared to influence the work reported in this paper.

Acknowledgments

The authors would like to acknowledge the DER-GOM srl company (www.dergom.com), involved in the study of the rubber compounds for the pads, the experimental testing of the pads and the production of the prototypes. In particular, Dr. Renato Cerchiaro is gratefully acknowledged.

References

[1] V.A. Matsagar, R.S. Jangid, Base isolation for seismic retrofitting of structures, Pract. Period. Struct. Des. Construct. 13 (4) (2008) 175.

[2] M. Mezzi, F. Comodini, L. Rossi, A base isolation option for the full seismic protection of an existing masonry school building, in: Proceedings of the Thirteenth International Conference on Civil, Structural and Environmental Engineering Computing, 2011.

[3] M.G. Melkumyan, Base isolation retrofitting design for the existing 9 story large panel apartment building, Int. J. Trends. Sci. Res.Dev. 4 (2020) 4.

[4] V.N. Thuyet, S.K. Deb, A. Dutta, Mitigation of seismic vulnerability of prototype low-rise masonry building using U-FREIs, J. Perform. Constr. Facil. 32 (2) (2018), 4017136.

[5] A.B. Habieb, F. Milani, G. Milani, R. Cerchiaro, Rubber compounds made of reactivated EPDM for fiber-reinforced elastomeric isolators: an experimental study, Iran. Polym. J. (Engl. Ed.) 29 (11) (2020) 1031–1043.

[6] A.B. Habieb, G. Milani, T. Tavio, F. Milani, Seismic protection of unreinforced masonry buildings by means of low cost elastomeric isolation systems, Int. J. Magn. Reson. Imag. 6 (2) (2021) 127–140.

[7] A.B. Habieb, M. Valente, G. Milani, Hybrid seismic base isolation of a historical masonry church using unbonded fiber reinforced elastomeric isolators and shape memory alloy wires, Eng. Struct. 196 (2019), 109281.

[8] A. Tsiavos, N.A. Alexander, A. Diambra, E. Ibraim, P.J. Vardanega, A. Gonzalez-Buelga, A. Sextos, A sand-rubber deformable granular layer as a low-cost seismic isolation strategy in developing countries: experimental investigation, Soil Dynam. Earthq. Eng. 125 (2019), 105731.

[9] A. Tsiavos, A. Sextos, A. Stavridis, M. Dietz, L. Dihoru, N.A. Alexander, Experimental investigation of a highly efficient, low-cost PVC-Rollers Sandwich (PVC-RS) seismic isolation, Structures 33 (2021) 1590–1602.

[10] A. Das, S.K. Deb, A. Dutta, Shake table testing of un-reinforced brick masonry building test model isolated by U-FREI, Earthq. Eng. Struct. Dynam. 45 (2) (2016) 253–272.

[11] A. Turer, B. Özden, Seismic base isolation using low-cost Scrap Tire Pads (STP), Mater. Struct. 41 (5) (2008) 891–908.

[12] R.P. Nanda, M. Shrikhande, P. Agarwal, Low-cost base-isolation system for seismic protection of rural buildings, Pract. Period. Struct. Des. Construct. 21 (1) (2016), 4015001.

[13] A.B. Habieb, G. Milani, R. Cerchiaro, V. Quaglini, F. Milani, Numerical study on rubber compounds made of reactivated ethylene propylene diene monomer for fiber reinforced elastomeric isolators, Polym. Eng. Sci. 61 (1) (2021) 258–277.

[14] E. Morales, A. Filiatrault, A. Aref, Sustainable and low cost room seismic isolation for essential care units of hospitals in developing countries, in: Proceeding of 16th World Conference on Earthquake Engineering. Santiago, 2017.

[15] N. Ahmad, H. Shakeel, M. Masoudi, Design and development of low-cost HDRBs seismic isolation of structures, Bull. Earthq. Eng. 18 (3) (2020) 1107–1138.

[16] M. Spizzuoco, A. Calabrese, G. Serino, Innovative low-cost recycled rubber-fiber reinforced isolator: experimental tests and Finite Element Analyses, Eng. Struct. 76 (2014) 99–111.

[17] A. Calabrese, M. Spizzuoco, G. Serino, G. Della Corte, G. Maddaloni, Shaking table investigation of a novel, low-cost, base isolation technology using recycled rubber, Struct. Control. Health Monit. 22 (2015) 107–122.

[18] B.Y. Moon, G.J. Kang, B.S. Kang, J.M. Kelly, Design and manufacturing of fiber reinforced elastomeric isolator for seismic isolation, J. Mater. Process. Technol. 130 (2002) 145–150.

[19] J. Kelly, Analysis of fiber-reinforced elastomeric isolators, J. Seismol. Earthq. Eng. 2 (1) (1999) 19–34.

[20] H. Toopchi-Nezhad, M.J. Tait, R.G. Drysdale, Lateral response evaluation of fiber-reinforced neoprene seismic isolators utilized in an unbonded application, J. Struct. Eng. 134 (10) (2008) 1627–1637.

[21] N.C. Van Engelen, P.M. Osgooei, M.J. Tait, D. Konstantinidis, Partially bonded fiber-reinforced elastomeric isolators (PB-FREIs), Struct. Control Health Monit. 22 (3) (2015) 417–432.

[22] A.B. Habieb, G. Milani, T. Tavio, Two-step advanced numerical approach for the design of low-cost unbonded fiber reinforced elastomeric seismic isolation systems in new masonry buildings, Eng. Fail. Anal. 90 (2018) 380–396.

[23] N.C. Van Engelen, D. Konstantinidis, M.J. Tait, Structural and nonstructural performance of a seismically isolated building using stable unbonded fiber-reinforced elastomeric isolators, Earthq. Eng. Struct. Dynam. 45 (3) (2016) 421–439.

[24] A.B. Habieb, M. Valente, G. Milani, Base seismic isolation of a historical masonry church using fiber reinforced elastomeric isolators, Soil Dynam. Earthq. Eng. 120 (2019) 127–145.

[25] G. Pianese, G. Milani, R. Cerchiaro, F. Milani, Optimal vulcanization of unbonded fiber reinforced elastomeric isolator devices, Chem. Eng. Trans. 86 (2021) 1321–1326.

[26] C. Guise-Richardson, Redefining vulcanization: charles goodyear, patents, and industrial control, 1834-1865, Technol. Cult. 51 (2) (2010) 357–387.

[27] G. Milani, F. Milani, Genetic algorithm for the optimization of rubber insulated high voltage power cables production lines, Comput. Chem. Eng. 32 (12) (2008) 3198–3212.

[28] G. Milani, F. Milani, Comprehensive numerical model for the interpretation of cross-linking with peroxides and sulfur: chemical mechanisms and optimal vulcanization of real items, Rubber Chem. Technol. 85 (4) (2012) 590–628.

[29] G. Milani, F. Milani, Parabola-Hyperbola PH kinetic model for NR sulphur vulcanization, Polym. Test. 58 (2017) 104–115.

[30] G. Milani, F. Milani, Curing degree prediction for S-TBBS-DPG natural rubber by means of a simple numerical model accounting for reversion and linear interaction, Polym. Test. 52 (2016) 9–23.

[31] G. Milani, F. Milani, Fast and reliable meta-data model for the mechanistic analysis of NR vulcanized with sulphur, Polym. Test. 33 (2014) 64–78.

[32] G. Milani, F. Milani, Optimal vulcanization of tires: experimentation on idealized NR-PB natural and poly-butadiene rubber blends, phenomenological smoothed numerical kinetic model and FE implementation, Polym. Test. 72 (2018) 63–85.

[33] Dassault Systemes, ABAQUS/Standard User's Manual, Version 6.13, Simulia Inc. (2020).

[34] G. Milani, F. Milani, Simple kinetic numerical model based on rheometer data for Ethylene–Propylene–Diene Monomer accelerated sulfur crosslinking, J. Appl. Poly. Sci. 14 (1) (2012) 311–324.

[35] ISO 7619-1:2010, International Standard on Rubber, Vulcanized or Thermoplastic — Determination of Indentation Hardness — Part 1: Durometer Method (Shore Hardness), 2010, 2010.

[36] ISO 37:2017, International Standard on Tensile Stress-Strain Properties, 2017, 2017.

[37] O.H. Yeoh, Some forms of the strain energy function for rubber, Rubber Chem. Technol. 66 (5) (1993) 754–771.

[38] P. Ghosh, A. Saha, P.C. Bohara, R. Mukhopadhyay, Material property characterization for finite element analysis of tires, Rubber World 233 (2006) 4.

[39] T. Chen, Determining Viscoelastic Strain Data a Prony Material Series for a from Time Varying, NASA Langley Research Center, Hampton, VA, USA, 2000.

[40] T. Dalrymple, J. Choi, K. Miller, Elastomer rate-dependence: a testing and material modeling methodology, in: 172nd Technical Meeting of the Rubber Division of the American Chemical Society (ACS), Cleveland, OH, 2007, pp. 16–18. Oct.

[41] M.A. Kraus, M. Schuster, J. Kuntsche, G. Siebert, J. Schneider, Parameter identification methods for visco-and hyperelastic material models, Glass. Struct. Eng. 2 (2) (2017) 147–167.